CONFERENCE PRE-PRINT

THE PHYSICS OF ELM-FREE REGIMES IN EUROFUSION TOKAMAKS *Pedestal tailoring via ballooning modes*

M.G. DUNNE, M. FAITSCH, A. KAPPATOU, J. HOBIRK, D. SILVAGNI, E. WOLFRUM

Max-Planck-Institute for Plasma Physics

Boltzmannstr. 2, 85748 Garching, Germany

Email: mike.dunne@ipp.mpg.de

O. SAUTER, B. LABIT

École Polytechnique Fédérale de Lausanne (EPFL), Swiss Plasma Center (SPC) CH-1015 Lausanne, Switzerland

E. VIEZZER

Dept. of Atomic, Molecular and Nuclear Physics

University of Seville, Spain

D. KEELING, E. LERCHE[†], P. LOMAS, I. BALBOA, D. KOS, S. SAARELMA,

S. SILBURN, H.J. SUN, A. TOOKEY

United Kingdom Atomic Energy Authority, Culham Science Centre

Abingdon, Oxon, OX14 3DB, United Kingdom of Great Britain and Northern Ireland

† also: Laboratory for Plasma Physics LPP-ERM/KMS, B-1000 Brussels, Belgium

B. VANOVAC

Plasma Science and Fusion Center, Massachusetts Institute of Technology Cambridge, MA 02139, United States of America

P. BILKOVA, P. BOHM

Institute of Plasma Physics of the CAS

Prague, Czech Republic

L. RADOVANOVIC

institute of Applied Physics, TU Wien, Fusion@ÖAW, Wiedner Hauptstr. 8-10, 1040 Vienna, Austria

E.R. SOLANO

Laboratorio Nacional de Fusión, CIEMAT

Spain

The ASDEX Upgrade Team

See the author list of H. Zohm et al, 2024 Nucl. Fusion https://doi.org/10.1088/1741-4326/ad249d

JET contributors

See the author list of C. Maggi et al, 2024 Nucl. Fusion https://doi.org/10.1088/1741-4326/ad3e16

The TCV Team

See author list of B.P. Duval et al. 2024 Nucl. Fusion https://doi.org/10.1088/1741-4326/ad8361

The EUROfusion Tokamak Exploitation Team

See the author list of E. Joffrin et al, 2024 Nucl. Fusion https://doi.org/10.1088/1741-4326/ad2be4

Abstract

The development of operational scenarios without large Type-I ELMs is of utmost importance for the stable operation and longevity of future tokamaks. The EUROfusion tokamak exploitation program has therefore made the understanding of ELM-free regimes a major topic of exploration across all its contributing devices (ASDEX Upgrade, JET, MAST-Upgrade, TCV, and WEST). An integrated program to investigate a range of Type-I ELM-free regimes has been developed covering the enhanced D-alpha (EDA), magnetic perturbations (MP), negative triangularity (NT), quasi-continuous exhaust (QCE),

quiescent H-mode (QH), the baseline small ELMs (SE), and X-point radiator (XPR) regimes. This contribution focuses on the development and understanding of the NT and QCE regimes on ASDEX Upgrade, JET, and TCV. The importance of transport via ballooning modes in both regimes is highlighted, as well as the progress in developing access models based on ideal-MHD. In the case of the QCE, this can also be expressed as a minimum separatrix density, which corresponds well to experimentally measured separatrix densities. Particular focus is paid to the performance of the QCE in terms of the achieved pedestal top values, which, when appropriately normalised, do not differ significantly from ELMy H-mode plasmas. This, combined with the predicted minimum separatrix density for the 15 MA ITER baseline plasma, highlight the relevance of the QCE as a potential operational scenario for both ITER and future reactors.

1. INTRODUCTION

The development of operational scenarios without large Type-I ELMs is of utmost importance for the stable operation and longevity of future tokamaks. To this end, one of the most important research topics at the moment is the search for robust ELM-free regimes with sufficient confinement to support a fusion reactor. The EUROfusion tokamak exploitation program has therefore made the understanding of ELM-free regimes a major topic of exploration across all its contributing devices (ASDEX Upgrade, JET, MAST-Upgrade, TCV, and WEST).

The overarching aim of the research topic is directed at the physics understanding of large-ELM-free regimes, rather than the development of an integrated high performance, detached ELM free scenario. The integration of a high performance core with an ELM-free pedestal and relevant divertor physics is quite challenging in present-day machines owing to the typical requirement of high separatrix density operation, which imposes known limitations on plasma performance[1, 2, 3]. Instead, the general approach of the topic is to investigate physics mechanisms in smaller, flexible devices, such as TCV and ASDEX Upgrade, to validate this understanding on a larger device (typically JET) and then use the validated physics mechanisms to make predictions for future devices such as SPARC and ITER.

A wide range of scenarios are being investigated across the different machines, covering the enhanced D-alpha (EDA)[4, 5], ELM suppression via magnetic perturbation (MP)[6, 7, 8], the I-mode[9], n the experimental time available.negative triangularity (NT)[10, 11, 12], the quasi-continuous exhaust (QCE) regime[13, 14, 15], quiescent H-mode (QH)[16, 17, 18, 19], the baseline small ELMs (SE), and X-point radiator (XPR) regimes[20]. The focus of this contribution is on the well-developed understanding of NT and QCE plasmas. A highlight of these efforts is the development and exploration of NT and QCE scenarios in JET, enabled via predictive modelling. A second highlight of the recent JET ELM-free experiments is the demonstration of both the QCE[21] and XPR[20] regimes in DT plasmas.

The manuscript is structured as follows: an introduction to a simple conceptual model of ELM-avoidance is presented, along with the tools which are used for modelling. The progress in developing ELM-free negative triangularity scenarios on ASDEX Upgrade and JET, following detailed experiments at TCV will be mentioned. The paper will, however, focus more on recent progress in the QCE regime, describing the current access model and a comparison of the scenario with ELMing H-modes on ASDEX Upgrade, JET, and TCV.

2. THE PHYSICS PICTURE OF TYPE-I ELM AVOIDANCE

The occurrence of Type-I ELMs can be understood as an intersection of transport in the pedestal (often considered to be a KBM[22]) determining the average pedestal gradient and the onset of a global peeling-ballooning mode. This is sketched in figure 1 as the red line, where the transport and MHD limits coincide. An experimental plasma is expected to exist on this red line, indicated by the star.

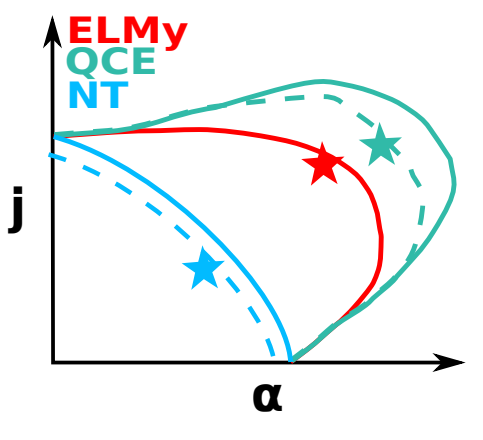


FIG. 1. Schematic of Type-I ELM avoidance for QCE (green) and NT (blue) plasmas vs an ELMy H-mode (red). The stars indicate the operational point expected in an experiment.

A large ELM crash can be avoided by tailoring both the transport and MHD limits. There are then two main categories of large-ELM avoidance: one applies to e.g. QCE and QH mode, where the Type-I ELM stability limit is raised (e.g. via increased plasma shaping) and additional transport is created via an MHD mode. This corresponds to the green lines in figure 1. In this case, the solid line indicates the global MHD stability limit, and the dashed line to the (slightly lower) transport limit. This allows an ELMy H-mode-like pedestal gradient to be sustained, shown by the green star, without the presence of large ELMs. A second type reduces both stability limits significantly, to the point where the H-mode is no longer accessed, as is the case in NT plasmas, corresponding

to the blue lines in figure 1; here, the star indicates the low expected pedestal gradient, which remains below the peeling-ballooning boundary.

The MHD limit and its dependencies are generally well understood; increasing the plasma shape, generally thought of as a combination of both elongation and triangularity[23], as well as the global plasma β [24] and q_{95} [25] tend to increase the stability limit. The main task of understanding the physics of ELM-free regimes is then one of understanding the transport mechanisms which regulate the pedestal gradient and the pedestal width.

2.1. Regions of the pedestal

The description of pedestal structure and transport in terms of only the pedestal height and width does not capture the finer details of the various transport mechanisms which can be present in the pedestal region. Gyrokinetic studies[26] of the ASDEX Upgrade pedestal have shown a range of instabilities which can be present at a given time. With this in mind, we can consider three regions of the pedestal: the top, close to the knee where the pedestal meets the core plasma; the middle, where the steepest gradients are located; and the foot, close to the separatrix.

QH-mode plasmas are well understood in the MHD framework; they rely on a saturated large-scale kink/peeling mode to provide extra transport. Recent modelling of a transient QH-mode phase in ASDEX Upgrade[27] has confirmed the physics picture, and highlighted the importance of low pedestal density in sustaining the QH-mode in these plasmas.

Previous studies[28] have posited the mechanism for ELM suppression via magnetic perturbations as being caused by the presence of an island at the pedestal top, blocking further expansion of the pedestal. An island has recently been observed in ELM-suppressed ASDEX Upgrade plasmas with magnetic perturbations[29].

Ballooning modes have been shown to play the dominant role in NT[11, 30] and QCE[31] plasmas. In the case of NT, H-mode avoidance has been linked with blocking access to the second stable region in s- α space[11], particularly in the middle region of the pedestal, where second-stability access is most likely. Access to the QCE is linked to keeping access to second-stability open in the middle of the pedestal and an unstable ballooning mode localised at the pedestal foot[13, 32, 33], independently of the structure of the rest of the pedestal (which may tend towards low-, medium-, or high-n modes).

3. SECOND STABILITY ACCESS: NEGATIVE TRIANGULARITY

The flexible shaping capabilities of TCV have helped drive the understanding of the separate elements of ELM-avoidance and confinement improvement in NT. Initial negative triangularity discharges at AUG showed no signs of ELM or H-mode avoidance[34, 35]. Since the original experiments the understanding of NT ELM avoidance[11, 30, 36] has developed, showing that blocking access to ballooning second stability avoids H-mode entry. These predictions indicated that minor changes to the AUG NT shape should be sufficient to block second stability access. In parallel, modelling also indicated that a negative triangularity shape which could be performed on the JET tokamak should also avoid H-mode access. Scaled versions of each of these shapes were developed on TCV and, combined with an NBI heating power ramp, verified H-mode avoidance in the range of relevant shapes.

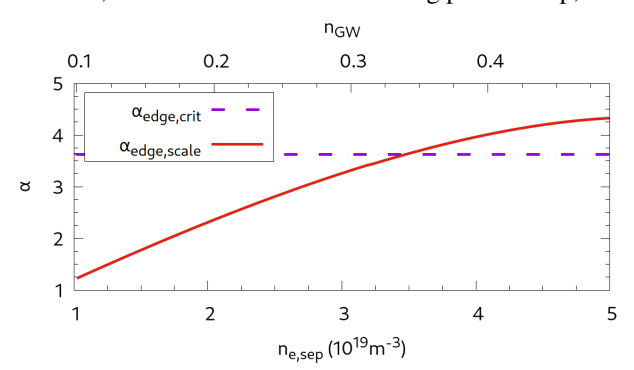


FIG. 2. Critical (purple) and expected (red) $\alpha_{\rm edge}$ vs $n_{\rm e,edge}$. The critical separatrix density is found at the intersection of both lines, above which one expects access to the QCE regime.

In the case of the JET shape, additional shaping scans at TCV to stronger negative shapes showed that, while the shaping requirements for ELM-avoidance were met, even more strongly shaped plasmas would have been necessary to see confinement improvement; this could not be tested due to limitations of the PF-coils at JET.

4. SEPARATRIX BALLOONING MODES: THE QUASI-CONTINUOUS EXHAUST REGIME

Recent understanding of the operational space of the QCE from the separatrix parameters[13, 15] and MHD stability[31, 23] helped guide the development of the QCE in JET[21, 37]; a sufficiently high shaping parameter (defined as $S_d = \kappa^{2.2}(1+\delta)^{0.9}$) and a critical separatrix density

which can be determined from machine parameters are the key requirements.

For a given plasma shape and q_{95} the critical $\alpha_{\rm edge}$ at the separatrix can be calculated using HELENA. This is typically done assuming a single value of the separatrix density, consistent with the standard EPED assumption.

Some change of the critical $\alpha_{\rm edge}$ could be expected depending on the form of the density profile and its subsequent impact on the bootstrap current and magnetic shear. However, given that $\alpha_{\rm edge}$ is located close to the separatrix, this is not expected to have a significant impact on the results. The resulting $\alpha_{\rm edge,crit}$ for an AUG scenario is shown as the horizontal dashed purple line in figure 3.

This critical $\alpha_{\rm edge}$ can be transformed into a critical $n_{\rm e,edge}$ as follows: an expected $\alpha_{\rm edge,exp}$ is constructed as ${\rm Rq^2}\beta/\lambda_{\rm p,scale}$ with $\beta \propto n_{\rm e,edge} T_{\rm e,edge}$. $T_{\rm e,edge}$ is determined from the input heating power and Spitzer-Harm conduction, while $n_{\rm e,edge}$ is used as a dependent parameter to scan. The final variable is $\lambda_{p,scale}$ which can be taken from a scaling of AUG discharges[38, 15] and is given as $1.55(1+0.61\alpha_t^{2.35})\rho_s$, where α_t is a collisional broadening parameter and ρ_s is the poloidal ion Larmor radius; all values are calculated self-consistently with the physical and magnetic geometry plus the power crossing the separatrix.

When comparing the predicted $\alpha_{\rm edge,crit}$ from HELENA and the expected $\alpha_{\rm edge,exp}$ it should be noted that the definitons are slightly different; HELENA uses the Miller definition of α [39], while the definition in this paragraph is a cylindrical approximation, with the simplification reflecting available experimental data.

This results in an expected $\alpha_{\rm edge}$ as shown by the red line in figure 2 for an ASDEX Upgrade scenario. The minimum density in this scenario is predicted to be $0.33 n_{\rm GW}$, with $n_{\rm GW} = I_{\rm p}({\rm MA})/(\pi a^2)(10^{20} {\rm m}^{-3})$. In the same way, predictions of the critical separatrix density can be made for any scenario on any device given only engineering parameters.

4.1. QCE access

The model described in the previous section posits access to the QCE regime at high shaping and high separatrix density. To test this on the three devices, an operational space of normalised separatrix density vs shaping parameter is shown for JET, AUG, and TCV in figure 3. A range of plasma current and toroidal field with different q₉₅ values in each device are shown. ELMy data points are shown as the red points, and QCE data as black points.

All experiments in JET shown here were performed with at a high fuelling rate and, hence, the separatrix density does not vary significantly across the data set. Instead, the plasma shape is the main dividing factor between ELMy and QCE data. In AUG and TCV the more typical picture

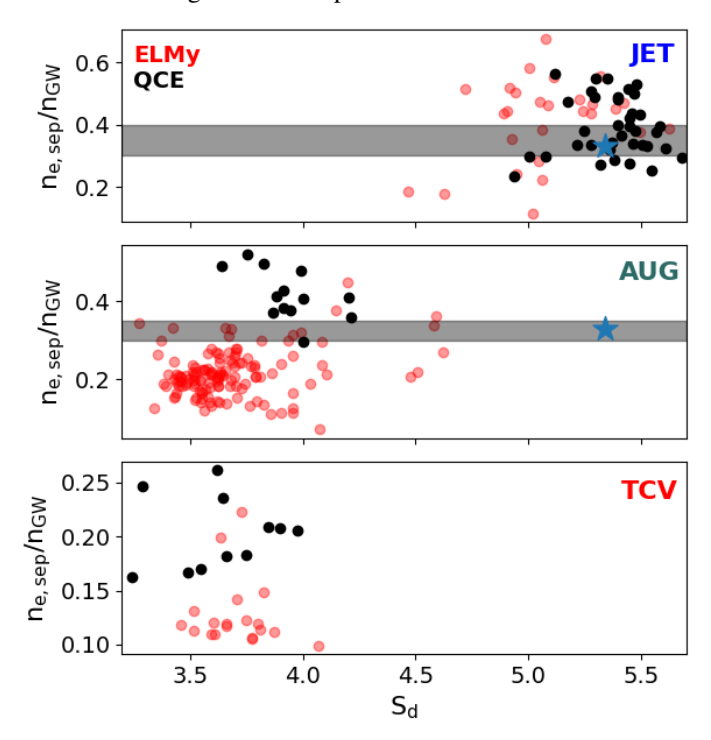


FIG. 3. Normalised separatrix density vs plasma shaping for a range of scenarios in (a) JET, (b) AUG, and (c) TCV. Red points indicate data from ELMy plasmas, while black indicates QCE phases. The horizontal grey box indicates the range of minimum normalised separatrix density for QCE access, while the stars show the predicted ITER minimum normalised density.

emerges with the QCE points existing at higher separatrix density. The grey boxes overlaying the JET and AUG data indicate the range of minimum predicted densities derived by the model from the previous section, which agrees well with the measured densities in both devices. Despite this, the model predicts separatrix densities far in excess of those observed in TCV; a solution is only found by removing the α_t dependence of the gradient lengths and lies at approximately $50\% n_{\rm GW}$. While the QCE does occur at higher density than the corresponding ELMy discharges, further investigations are necessary to explain the onset of QCE.

Also overlayed on the AUG and JET data is a blue star indicating the predicted minimum separatrix Greenwald fraction for ITER at the ITER shape[23]. This shows that not only is the QCE predicted for ITER, but that the ITER shaping has already been tested at JET, and the normalised and absolute separatrix densities for QCE entry in ITER has already been achieved in AUG and JET. The QCE can therefore be expected to be accessible in ITER, as its entry requirements are met by the expected operating conditions of the device (medium-high separatrix density and high plasma shaping)[40].

4.2. Pedestal performance

Of particular interest for projection of the QCE regime to future devices are conditions at the pedestal top. With this in mind, figure 4 compares the pedestal top temperature and density for JET, AUG, and TCV in QCE and ELMing plasmas for the same scenarios shown in figure 3.

Since a range of plasma currents, magnetic fields, plasma shapes, and q_{95} values are considered, a fair comparison is best made by normalising the pedestal top values. A natural choice for the density is to normalise it to the Greenwald density. For the temperature, a normalisation to I_p/κ^2 , with kappa being the elongation, can be considered; this renders the "isobars" (dashed grey lines) in figure 4 lines of constant $\beta_{e,pol,ped}$, the electron pedestal top poloidal β . The plot ordering and color scheme are the same as in figure 3. The dashed grey lines in all three subplots show the same $\beta_{pol,ped}$ values (0.08 and 0.2), indicating that the same range of $\beta_{e,pol,ped}$ values are obtained in all three devices.

With this choice of normalisation, no difference between ELMy H-mode pedestal top values and those in the QCE regime can be discerned. In fact, the JET data completely overlap in the two regimes, not only in β but also in the normalised temperature and density. The AUG and TCV data exist, as might be expected, at higher normalised pedestal top density. The AUG data are quite beneficial in this comparison as they cover quite a wide range of plasmas, including those aimed at reaching low collisionality. With this in mind, it is interesting to note that the QCE still exists in the same $\beta_{e,pol,ped}$ range.

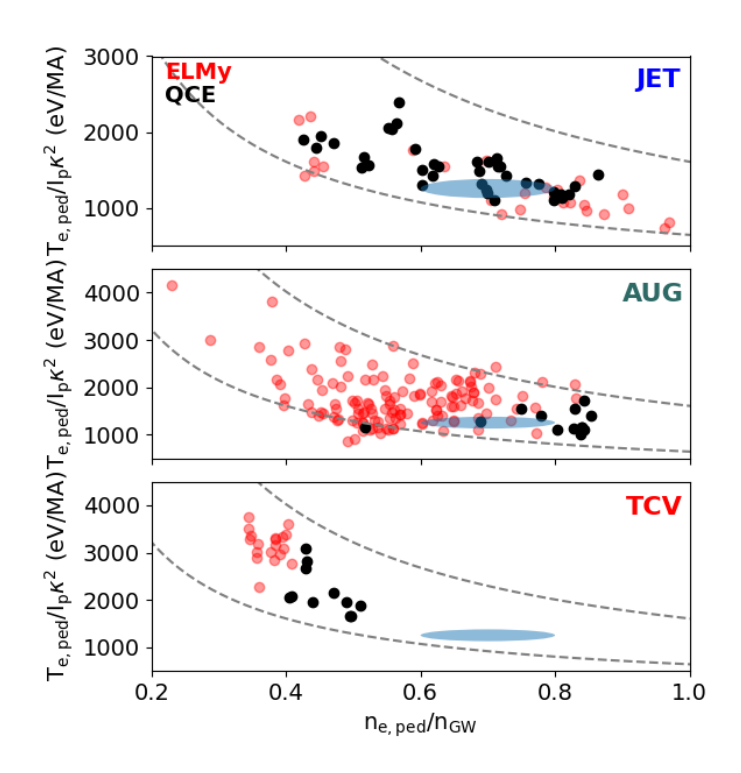


FIG. 4. Normalised pedestal top temperature vs density for (a) JET, (b) AUG, and (c) TCV in QCE (black) and ELMy (red) plasmas. The isobars (dashed grey) indicate lines of constant $\beta_{e,pol,ped}$ with values of 0.08 and 0.2 for each device.

Finally, the blue ellipses overlayed on the three plots indicate a range of expectations for the ITER 15 MA baseline pedestal, with a Greenwald fraction between 0.6-0.8, and an expected pedestal top temperature of 4-5.5 keV, again demonstrating the compatibility of the ITER pedestal with the QCE regime. The AS-DEX Upgrade and JET data overlap in both normalised temperature and density, while the TCV data exist at lower normalised density. The compatibility of ITER and high pedestal performance in conjunction with the existence of edge ballooning modes has also been shown in several other works[41, 31, 42].

4.3. The QCE in DT at JET

The successful demonstration of the QCE in DT at JET has already been reported[21, 43], highlighting the easy transfer of the scenario from D to DT operation. The confinement improvement, often observed in ELMy H-modes when switching to DT operation was also observed in the QCE. Figure 5 shows the pedestal top temperature and density (both without normalisation) for two JET QCE scenarios at 1.5 MA (stars) and 2.0 MA (squares), each with a

 q_{95} of 4.0, for D (blue) and DT (gold) plasmas. The increase of pedestal density at constant temperature with increasing plasma current is clear. Also clear is the increase in pedestal top pressure, mainly coming from an increase in density when changing from D to DT plasmas, as has been already reported[21].

Overlayed on figure 5 are green shapes corresponding to IPED predictions for the pedestal height in each of the scenarios. These predictions were made with the "standard" width pre-factor of 0.076[22], and so represent a conservative estimate for the pedestal height while underestimating the pedestal width. Nevertheless, this indicates that the pedestal in QCE plasmas is broadly consistent with the predictions for an ELMy H-mode pedestal.

4.4. Extrapolation to ITER

The ability to predict the minimum separatrix density and expected pedestal top density in the QCE regime using ideal MHD lends further support to the QCE as a plasma scenario for ITER. Previous work[41, 31, 42] has indicated that ballooning modes are expected in the pedestal of the 15 MA baseline scenario, while maintaining high pedestal top temperature and pressure. Recent work[23] has also shown that the minimum separatrix density required for QCE access in ITER is approximately 30%n_{GW}, which is in the range of densities achieved in present-day machines. While the normalised global confinement time in QCE scenarios is often below 1.0, the pedestal performs as expected by ideal MHD, meaning that an integrated modelling code, such as IMEP[42], can make better predictions when extrapolating a high density scenario, such as the QCE.

5. SUMMARY AND CONCLUSIONS

The work presented here has shown the current understanding of the physics mechanisms for access to the QCE and NT large ELM-avoidance regimes. In both cases, ballooning modes play a dominant role. For the QCE, a ballooning mode at the separatrix (modelled using an ideal ballooning mode and in reality, likely a KBM of some kind), while for NT blocking access to second stability in the middle of the pedestal is a requirement for avoiding large ELMs. The understanding gained from experiments across both EUROfusion and other international devices allows predictions to be made, making scenario development on devices significantly easier.

The stepladder approach within EUROfusion, understanding physics on smaller devices before applying it to larger ones, notably JET, has significantly shortened scenario development time necessary for both QCE and NT demonstration in JET; without guidance from modelling and experimental validation on AUG and TCV, neither the QCE nor NT would have been possible in the experimental time available. The successful demonstration of the QCE in D plasmas in JET also paved the way for a successful series of QCE experiments in DT plasmas. This important step highlights that the lessons learned during non-nuclear phases can be easily transferred to DT operation in future devices. Predictions for the minimum density for QCE access in ITER indicate that the regime will be accessible in ITER, and pedestal predictions made with ideal MHD codes are also expected to apply in the QCE regime in ITER. SPARC and EU-DEMO-like tokamaks are also expected to easily access the QCE regime owing to the large poloidal field in these devices.

NT ELM avoidance has been successfully demonstrated on both AUG and JET, guided by modelling and similarity experiments in TCV. Since the minimum shaping required can be predicted by ideal MHD, the required triangularity for any future devices can also be predicted, and tested on currently running machines to further validate the model.

Work is still ongoing in the EUROfusion program to extend not only the QCE and NT regimes to other devices, but also the EDA H-mode, I-mode, MP ELMsuppression, and QH-mode. The expansion of the QCE operational range to higher current and even lower $q_{95}(<3.5)$ than has already been achieved[21] has a high priority. While it has been shown for a single plasma[15], robust ELM avoidance during the current ramp and across the LH transition is also a high priority for future experiments; with guidance from modelling, significant progress in feedback control of such experiments is expected. Finally, the plasma-wall interaction in QCE plasmas must also be understood, as the fall-off lengths in the SOL become significantly longer than in ELMy H-mode plasmas[44, 45] and may increase the first-wall loads.

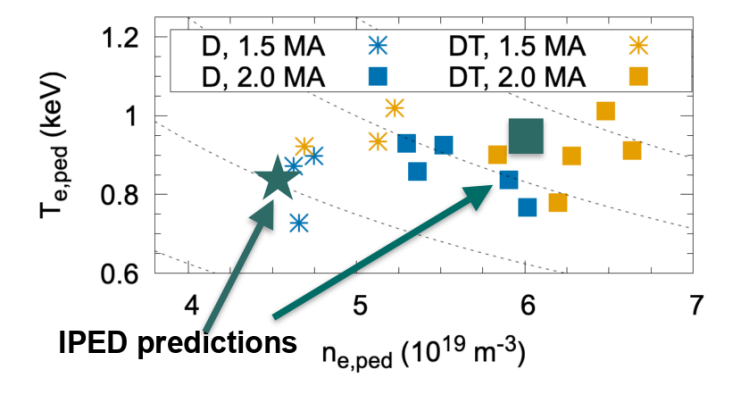


FIG. 5. Temperature vs density for two JET QCE scenarios at 1.5 MA (stars) and 2 MA (squares) in D (blue) and DT (gold) operation. The green shapes correspond to IPED predictions for the pedestal height in both scenarios.

The final test of the OCE regime will come with the next generation of devices which are currently being commissioned and built; JT-60SA, SPARC, and DTT. These devices will allow a more complete test of core-edge integration than is possible with current devices, in particular the combination of the high separatrix density and collisionality required for power exhaust with the low pedestal top collisionality expected in high fusion gain scenarios. Modelling has allowed predictions to be made for future devices, and the validation efforts taking place on present-day machines will allow targeted scenario development, as was displayed during the JET experiments. Combined with integrated models, the physics of ELM-free regimes can be better projected to future devices, ensuring safe machine operation, while fulfilling their fusion power mission.

ACKNOWLEDGEMENTS

This work has been carried out within the framework of the EUROfusion Consortium, partially funded by the European Union via the Euratom Research and Training Programme (Grant Agreement No 101052200 — EU-ROfusion). The Swiss contribution to this work has been funded by the Swiss State Secretariat for Education, Research and Innovation (SERI). Views and opinions expressed are however those of the author(s) only and do not necessarily reflect those of the European Union, the European Commission or SERI. Neither the European Union nor the European Commission nor SERI can be held responsible for them.

REFERENCES

- [1] M.G. Dunne, et al. The role of the density profile in the ASDEX-Upgrade pedestal structure. *Plasma Physics and Controlled Fusion*, 59, 2017.
- [2] L. Frassinetti, et al. Pedestal structure, stability and scalings in JET-ILW: The EUROfusion JET-ILW pedestal database. *Nuclear Fusion*, 61, 2021.
- [3] U A Sheikh, et al. Pedestal structure and energy confinement studies on TCV. *Plasma Physics and Controlled Fusion*, 61(1), nov 2018.
- [4] M. Greenwald, et al. Characterization of enhanced D high-confinement modes in Alcator C-Mod. *Physics of Plasmas*, 6(5), May 1999. _eprint: https://pubs.aip.org/aip/pop/article-pdf/6/5/1943/19073048/1943_1_online.pdf.
- [5] L. Gil, et al. EDA H-mode in ASDEX Upgrade: scans of heating power, fueling, and plasma current. *Nuclear Fusion*, 65(4), mar 2025.
- [6] T E Evans, et al. Suppression of Large Edge-Localized Modes in High-Confinement. Physical Review Letters, 92, 2004.
 NULL.
- [7] R. Nazikian, et al. Pedestal Bifurcation and Resonant Field Penetration at the Threshold of Edge-Localized Mode Suppression in the DIII-D Tokamak. *Phys. Rev. Lett.*, 114, Mar 2015.
- [8] W. Suttrop, et al. Experimental studies of high-confinement mode plasma response to non-axisymmetric magnetic perturbations in ASDEX Upgrade. *Plasma Physics and Controlled Fusion*, 59, 2017.
- [9] A.E. Hubbard, et al. Multi-device studies of pedestal physics and confinement in the I-mode regime. *Nuclear Fusion*, 56(8), jul 2016.
- [10] A. Marinoni, et al. A brief history of negative triangularity tokamak plasmas. Reviews of Modern Plasma Physics, 5(1), October 2021.
- [11] A.O. Nelson, et al. Prospects for H-mode inhibition in negative triangularity tokamak reactor plasmas. *Nuclear Fusion*, 62, 2022.
- [12] S. Coda, et al. Enhanced confinement in diverted negative-triangularity L-mode plasmas in TCV. *Plasma Physics and Controlled Fusion*, 64, 2021.
- [13] GF Harrer, et al. Parameter dependences of small edge localized modes (ELMs). Nuclear Fusion, 58, 2018.
- [14] B Labit, et al. Dependence on plasma shape and plasma fueling for small edge-localized mode regimes in TCV and ASDEX Upgrade. *Nuclear Fusion*, 59, 8 2019.
- [15] M. Faitsch, et al. Analysis and expansion of the quasi-continuous exhaust (QCE) regime in ASDEX Upgrade. *Nuclear Fusion*, 63(7), may 2023.
- [16] K H Burrell, et al. Quiescent H-mode plasmas in the DIII-D tokamak. Plasma Physics and Controlled Fusion, 44(5A), apr 2002.
- [17] W Suttrop, et al. Study of quiescent H-mode plasmas in ASDEX Upgrade. *Plasma Physics and Controlled Fusion*, 46(5A), apr 2004.
- [18] W. Suttrop, et al. Studies of the 'Quiescent H-mode' regime in ASDEX Upgrade and JET. *Nuclear Fusion*, 45(7), jul 2005.
- [19] Xi Chen, et al. Expanding the parameter space of the wide-pedestal QH-mode towards ITER conditions. *Nuclear Fusion*, 60(9), aug 2020.
- [20] M. Bernert, et al. X-point radiation: From discovery to potential application in a future reactor. *Nuclear Materials and Energy*, 43, 2025.
- [21] M. Faitsch, et al. The quasi-continuous exhaust regime in JET. *Nuclear Fusion*, 65, 2025.
- [22] P. B. Snyder, et al. Development and validation of a predictive model for the pedestal height. *Physics of Plasmas*, 16, 2009.

- [23] M. Dunne, et al. Quasi-continuous exhaust operational space. Nuclear Fusion, 64, 2024.
- [24] M.G. Dunne. Impact of impurity seeding and divertor conditions on transitions, pedestal structure and ELMs. *Nuclear Fusion*, 57, 2017.
- [25] P.B. Snyder, et al. High fusion performance in Super H-mode experiments on Alcator C-Mod and DIII-D. *Nuclear Fusion*, 59(8), jun 2019.
- [26] L.A. Leppin, et al. Complex structure of turbulence across the ASDEX Upgrade pedestal. *Journal of Plasma Physics*, 89(6), 2023.
- [27] Lorenz Meier, et al. MHD simulations of formation, sustainment and loss of quiescent H-mode in the all-tungsten ASDEX Upgrade. *Nuclear Fusion*, 63(8), jul 2023.
- [28] P. B. Snyder, et al. The EPED pedestal model and edge localized mode-suppressed regimes: Studies of quiescent H-mode and development of a model for edge localized mode suppression via resonant magnetic perturbations. *Physics of Plasmas*, 19, 2012.
- [29] M. Willensdorfer, et al. Observation of magnetic islands in tokamak plasmas during the suppression of edge-localized modes. *Nature Physics*, 20(12), Dec 2024.
- [30] A. O. Nelson, et al. Robust Avoidance of Edge-Localized Modes alongside Gradient Formation in the Negative Triangularity Tokamak Edge. *Phys. Rev. Lett.*, 131, Nov 2023.
- [31] L. Radovanovic, et al. Developing a physics understanding of the quasi-continuous exhaust regime: Pedestal profile and ballooning stability analysis. *Nuclear Fusion*, 62, 8 2022.
- [32] M. Griener, et al. Continuous observation of filaments from the confined region to the far scrape-off layer. *Nuclear Materials and Energy*, 25, 2020.
- [33] J. Kalis, et al. Experimental characterization of the quasi-coherent mode in EDA H-Mode and QCE scenarios at ASDEX Upgrade. *Nuclear Fusion*, 64(1), dec 2023.
- [34] T. Happel, et al. Overview of initial negative triangularity plasma studies on the ASDEX Upgrade tokamak. *Nuclear Fusion*, 63(1), nov 2022.
- [35] B Vanovac, et al. Pedestal properties of negative triangularity discharges in ASDEX Upgrade. *Plasma Physics and Controlled Fusion*, 66(11), sep 2024.
- [36] O. Sauter et al. Negative triangularity tokamak operation in TCV, IAEA FEC 2023. 2023.
- [37] M. Faitsch, et al. The quasi-continuous exhaust regime in ASDEX Upgrade and JET. Nuclear Materials and Energy, 42, 2025.
- [38] T. Eich, et al. Turbulence driven widening of the near-SOL power width in ASDEX Upgrade H-Mode discharges. *Nuclear Fusion*, 60, 2020.
- [39] R. L. Miller, et al. Noncircular, finite aspect ratio, local equilibrium model. *Physics of Plasmas*, 5, 1998.
- [40] A.A. Pshenov, et al. SOLPS-ITER simulations of the ITER divertor with improved plasma-facing component geometry. *Nuclear Materials and Energy*, 42, 2025.
- [41] P. Maget, et al. MHD stability of the pedestal in ITER scenarios. Nuclear Fusion, 53, 2013.
- [42] T. Luda, et al. Effect of the plasma size on pedestal and global confinement and prediction for ITER with IMEP. *Nuclear Fusion*, 65(7), jun 2025.
- [43] A Kappatou, et al. Overview of the third JET deuterium-tritium campaign. Plasma Physics and Controlled Fusion, 67(4), apr 2025.
- [44] A. Redl, et al. An extensive analysis of SOL properties in high-d plasmas in ASDEX Upgrade. *Nuclear Fusion*, 64(8), jul 2024.
- [45] H.J. Sun, et al. Impact of the plasma boundary on machine operation and the risk mitigation strategy on JET. *Nuclear Fusion*, 65(7), jun 2025.